MONTE CARLO SIMULATION OF NEUTRAL BEAM INJECTION IN THE WENDELSTEIN VII-A STELLARATOR

H. Maaßberg

IPP 2/281 June 1986

MAX-PLANCK-INSTITUT FÜR PLASMAPHYSIK

8046 GARCHING BEI MÜNCHEN

MAX-PLANCK-INSTITUT FÜR PLASMAPHYSIK

GARCHING BEI MÜNCHEN

MONTE CARLO SIMULATION OF NEUTRAL BEAM INJECTION IN THE WENDELSTEIN VII-A STELLARATOR

H. Maaßberg

IPP 2/281 June 1986

Die nachstehende Arbeit wurde im Rahmen des Vertrages zwischen dem Max-Planck-Institut für Plasmaphysik und der Europäischen Atomgemeinschaft über die Zusammenarbeit auf dem Gebiete der Plasmaphysik durchgeführt.

MONTE CARLO SIMULATION OF NEUTRAL BEAM INJECTION IN THE WENDELSTEIN VII-A STELLARATOR

H. Maaßberg

Max-Planck-Institut für Plasmaphysik
Association EURATOM-IPP
Garching bei München
Federal Republic of Germany

Abstract

Strong neutral beam heating in the W VII-A stellarator with injection nearly perpendicular to the magnetic field results in a high energy ion tail. In a simplified model, the full nonlinear Fokker-Planck equation based on Coulomb interactions is solved self-consistently by means of Monte Carlo techniques. Generalized scattering operators which are equivalent to the nonlinear Fokker-Planck collision term are derived. With the numerical simulation, the strong neutral beam heating is analyzed for a typical discharge in W VII-A with H^o injection in a H^+/D^+ plasma mixture for stationary conditions. Both deuterium and hydrogen distribution functions are calculated. The D^+ distribution is found to be highly isotropic, the deviation from a Maxwellian resulting mainly from electron cooling. Furthermore, ion heat conduction is of minor importance for the energy balance of the bulk part of the plasma. The H^+ distribution, however, develops a strong pressure anisotropy, which can also be deduced experimentally from the diamagnetic signal.

I. Introduction

For typical currentless discharges in the W VII-A stellarator ($R = 200\ cm$, $r_a = 10\ cm$, $l = 2$, $m = 5$), heated by 3 or 4 neutral beam lines ($27\ kV$, H^o or D^o in D^+-target plasma, $80 - 120\ kW$ absorbed power per injector, nearly perpendicular to B (84^o)), the ion temperature ($400\ eV \leq T_i \leq 1000\ eV$) exceeds the electron temperature /1/, /2/.

The heating efficiency of the nearly perpendicular neutral beam injection (NBI) and the fast particle slowing-down in W VII-A have been central problems during the last few years. With injection of deuterium instead of hydrogen and with highly time-resolved measurements during the switch-off phase of the injectors, the heating mechanism can now be understood. The earlier hypothesis of very fast slowing-down with preferential ion heating related to ion cyclotron instabilities driven by the nearly perpendicular NBI could not be verified. In the deuterium injection experiments, the measured neutron flux of D^+-D^+ reactions both in the stationary and transient phase after switch-off of the D^o-injector agree very well with theoretical predictions based on the assumption of Coulomb collisions /3/. Energy analysis of the charge exchange (CX) neutrals of the H^+ slowing-down distribution leads to the same conclusion /4/. By linear stability analysis of the slowing-down distribution function calculated with the assumption of Coulomb interactions, no significant ion cyclotron instabilities were found for stationary conditions /5/,/6/.

Strong radial electric fields had been derived from the poloidal plasma rotation measured by Doppler shift of impurity lines. The particle confinement of both the thermal ions and the fast ions of the NBI is significantly improved by these fields. Then, the ion energy balance is determined mainly by the beam power transferred to the ions (which is less than the part transferred to the electrons) and by electron cooling (T_e is less than T_i in almost all cases). Ion heat conduction is of minor importance for the bulk part of the plasma /7/. In case of collisional slowing-down, the high-power nearly perpendicular NBI is connected with a strong pressure anisotropy which results from the distribution function of the beam particles. Furthermore, deviations in the thermal D^+ distribution (in the case of H^o injection) may be expected due to collisions of D^+ particles with the strongly anisotropic H^+ distribution. The evaluation of the ion temperature by energy analysis of the charge exchange deuterium neutrals in the range of $2T_i \leq E \leq 7T_i$ is very sensitive to distortions of the D^+ distribution function perpendicular to B.

The aim of this report is to describe the ion distribution functions in the case of strong NBI and to estimate the pressure anisotropy. In a simplified model (homogeneous in configuration space), the full nonlinear Fokker-Planck equation describing the Coulomb interactions is solved by means of Monte Carlo simulation. In the past, different methods have been developed to solve this nonlinear system of partial differential equations for all distribution functions (see e.g. /8/ and /9/), most of them based on finite difference schemes and/or eigenfunction expansion. The Monte Carlo simulation technique, however, seems to have been applied only to the linearized problem of test particles in an isotropic

Maxwellian background. Since the Monte Carlo simulation technique becomes very important in calculating the plasma transport /10/, /11/, /12/ as well as the heating efficiency and power deposition of neutral beam heated plasmas /13/, the simulation technique is extended to the full nonlinear problem in this report. Generalized scattering operators are derived with the random process unspecified. For the calculations described in this report, Gaussian random processes are used.

The Monte Carlo simulation is applied to the case of strong neutral beam heating with H^o injection into a H^+-D^+ plasma mixture. Neglecting fast orbit losses and ion heat conduction, an upper limit of the ion temperature is calculated for both NBI heating power and electron temperature given. Furthermore, the distortion of the D^+ distribution function and the slowing-down distribution function (H^+) is evaluated. Finally, experimental results for the deuterium temperature, the pressure anisotropy and the high energy H^+-spectrum are discussed.

II. Basic Equations

The magnetic field is assumed to be constant, and a configuration space dependence of the distribution functions is disregarded. For collision frequencies small compared to the cyclotron frequencies, the model becomes axisymmetric in velocity space with respect to the magnetic field, $\underline{B}$. Then, the Fokker-Planck equation can be written in the form given by Rosenbluth et al. /14/ :

$$\frac{\partial f_\alpha}{\partial t} = \Gamma_\alpha \cdot \frac{1}{v^2} \cdot \left[\frac{\partial}{\partial v}(A_1 f_\alpha) + \frac{1}{2}\frac{\partial^2}{\partial v^2}(A_2 f_\alpha) + \frac{\partial^2}{\partial v \partial p}(C f_\alpha) + \frac{\partial}{\partial p}(B_1 f_\alpha) + \frac{1}{2}\frac{\partial^2}{\partial p^2}(B_2 f_\alpha) \right] + S_\alpha \qquad (1)$$

Here, f_α is the distribution function of species α, v the absolute value of the velocity, p the pitch ($v_\parallel / v$) and S_α the particle source (and loss) term,

$$\Gamma_\alpha = \frac{\ln \Lambda}{4\pi} \cdot \left(\frac{Z_\alpha e^2}{\epsilon_o m_\alpha} \right)^2 ,$$

with $\ln \Lambda$ being the Coulomb logarithm, Z_α the charge number, and m_α the mass of the particles of species α. The coefficient functions A_1, A_2, B_1, B_2 and C in eq. (1) are defined by derivatives of the Rosenbluth potentials h_α and g:

$$A_1 = -v^2 \frac{\partial h_\alpha}{\partial v} - \frac{\partial g}{\partial v} - \frac{1}{2v}\frac{\partial}{\partial p}(1-p^2)\frac{\partial g}{\partial p}$$

$$A_2 = v^2 \frac{\partial^2 g}{\partial v^2}$$

$$B_1 = -(1-p^2)\frac{\partial h_\alpha}{\partial p} + \frac{1}{2v}\left\{(1-p^2)\left(\frac{p}{v}\frac{\partial^2 g}{\partial p^2} + 2\frac{\partial^2 g}{\partial v \partial p}\right) + 2p\frac{\partial g}{\partial v} - \frac{2}{v}\frac{\partial g}{\partial p}\right\}$$

$$B_2 = \frac{1-p^2}{v}\left\{\frac{1-p^2}{v}\frac{\partial^2 g}{\partial p^2} + \frac{\partial g}{\partial v} - \frac{p}{v}\frac{\partial g}{\partial p}\right\}$$

$$C = (1-p^2)\left\{\frac{\partial^2 g}{\partial v \partial p} - \frac{1}{v}\frac{\partial g}{\partial p}\right\}. \qquad (2)$$

The Rosenbluth potentials h_α and g are defined by the differential equations:

$$\Delta h_\alpha = -4\pi \sum_\beta Z_\beta^2 \left(1 + \frac{m_\alpha}{m_\beta}\right) f_\beta$$

$$\Delta\Delta g = -8\pi \sum_\beta Z_\beta^2 f_\beta, \qquad (3)$$

where Δ is the Laplace operator. Here, the summation is carried out with respect to all plasma species β. Alternatively, h_α and g can be defined by the explicit formulas:

$$h_\alpha = \sum_\beta Z_\beta^2 \left(1 + \frac{m_\alpha}{m_\beta}\right) \int_{-\infty}^{+\infty} \int \frac{1}{|\underline{v} - \underline{v}'|} f_\beta(\underline{v}')\, d^3 v'$$

$$g = \sum_\beta Z_\beta^2 \int_{-\infty}^{+\infty} \int |\underline{v} - \underline{v}'|\, f_\beta(\underline{v}')\, d^3 v'. \qquad (4)$$

For large values of the velocity, h_α converges as $1/v$, whereas g diverges as v. In the differential form of eq. (3), the boundary values are defined at infinity. Consequently, instead of using fast Poisson solvers, the Rosenbluth potentials h_α and g and all derivatives in eq. (2) are calculated from the explicit formulas (4) by means of Legendre expansion of the distribution functions f_β (see Appendix A1). For f_β being Maxwellians, the Rosenbluth potentials and the coefficient functions in the Fokker-Planck equation can be calculated analytically (see Appendix A2).

To derive the scattering operators for the Monte Carlo simulation, moment equations are calculated directly from the Fokker-Planck equation. Let $\langle v^l p^k \rangle_\alpha$ be the moments defined by

$$\langle v^l p^k \rangle_\alpha = \frac{2\pi}{n_\alpha} \int_0^\infty \int_{-1}^1 v^l p^k f_\alpha v^2\, dp\, dv,$$

where n_α is the particle density. Straightforward calculation with integration by parts yields

$$\frac{1}{\Gamma_\alpha}\frac{d}{dt}\langle v^l p^k\rangle_\alpha = -\,l\langle v^{l-3}p^k A_1\rangle_\alpha + \frac{l(l-1)}{2}\langle v^{l-4}p^k A_2\rangle_\alpha$$
$$- k\langle v^{l-2}p^{k-1}B_1\rangle_\alpha + \frac{k(k-1)}{2}\langle v^{l-2}p^{k-2}B_2\rangle_\alpha$$
$$+ l\cdot k\langle v^{l-3}p^{k-1}C\rangle_\alpha + \frac{2\pi}{\Gamma_\alpha n_\alpha}\int_0^\infty\int_{-1}^{1} v^l p^k\, S_\alpha\, v^2\, dp\, dv. \qquad (5)$$

III. Monte Carlo Scattering Operator

In the Monte Carlo simulation, the distribution function f_α is represented by an ensemble of simulation particles (test particle model). The scattering operators for the simulation particles are functions of the Rosenbluth potentials, which on the other hand depend on all distribution functions f_β. Consequently, this nonlinear problem is solved by iteration as is well known for Monte Carlo techniques. Within the iteration, the distribution function f_α is estimated in a velocity space mesh from the number of simulation particles of species α within the mesh cells. For stationary conditions, the statistical accuracy can be significantly improved by means of a time average. From the f_α, the Rosenbluth potentials are calculated directly (s. Appendix A1) for the next iteration step. This procedure leads to a field particle model for the Coulomb scattering of each simulation particle.

The Fokker-Planck equation (1) describes the diffusion in velocity space of each simulation particle including generation as well as annihilation as defined by the particle source term S_α. The Coulomb scattering is approximated by a sequence of random processes with random changes of the velocities of the simulation particles, these changes Δv and Δp being related to small time steps Δt. Then, the equivalent Monte Carlo scattering operator is defined as the single random process in v and p depending on Δt and including conservation of the simulation particles. The particle source term S_α is modelled independently.

The random process is characterized by the expectation values which must be consistent with the moment equations (5). For estimating the scattering operators, the particle source term S_α in (5) is disregarded. The corresponding expectation values up to second order are defined by the moment equations:

$$\frac{d}{d\tau}\langle v\rangle_\alpha = -\left\langle\frac{A_1}{v^2}\right\rangle_\alpha$$
$$\frac{d}{d\tau}\langle p\rangle_\alpha = -\left\langle\frac{B_1}{v^2}\right\rangle_\alpha$$

$$\frac{d}{d\tau}\langle v^2\rangle_\alpha = -2\left\langle\frac{A_1}{v}\right\rangle_\alpha + \left\langle\frac{A_2}{v^2}\right\rangle_\alpha$$
$$\frac{d}{d\tau}\langle p^2\rangle_\alpha = -2\left\langle\frac{pB_1}{v^2}\right\rangle_\alpha + \left\langle\frac{B_2}{v^2}\right\rangle_\alpha$$
$$\frac{d}{d\tau}\langle v\,p\rangle_\alpha = -\left\langle\frac{pA_1}{v^2}\right\rangle_\alpha - \left\langle\frac{B_1}{v}\right\rangle_\alpha + \left\langle\frac{C}{v^2}\right\rangle_\alpha, \tag{6}$$

with the abbreviation $\tau = \Gamma_\alpha \cdot \Delta t$. For small time increments Δt, the probability distribution of the random scattering process for each simulation particle is highly localized in velocity space. Therefore, the moments on the right side in equations (6) can be replaced by use of the initial values v_i, p_i of the simulation particle i (the index α of the plasma species is omitted in the following). Integration of equations (6) yields to 1st order in time:

$$\langle v\rangle = v_i - \frac{A_1}{v_i^2}\cdot\tau$$
$$\langle p\rangle = p_i - \frac{B_1}{v_i^2}\cdot\tau$$
$$\sigma_v^2\cdot\tau = \langle v^2\rangle - \langle v\rangle^2 = \frac{A_2}{v_i^2}\cdot\tau$$
$$\sigma_p^2\cdot\tau = \langle p^2\rangle - \langle p\rangle^2 = \frac{B_2}{v_i^2}\cdot\tau$$
$$\gamma\cdot\sigma_v\sigma_p\cdot\tau = \langle v\,p\rangle - \langle v\rangle\langle p\rangle = \frac{C}{v_i^2}\cdot\tau. \tag{7}$$

Here, the coefficient functions A_1, A_2, B_1, B_2 and C are defined at the initial values v_i, p_i of the simulation particle i. The standard deviations $\sigma_v\sqrt{\tau}$ and $\sigma_p\sqrt{\tau}$ of the random process must be very small compared to the domains of definition for v and p since the moments (eqs. 7) are only valid to first order in Δt. This leads to the limiting condition

$$\Delta t \ll \min\Big\{\frac{v_i^4}{A_2\,\Gamma}\,,\ \frac{v_i^2}{B_2\,\Gamma}\Big\}. \tag{8}$$

From this point on, the form of the random process must be specified. The two-dimensional random process can be separated after transformation to the statistically independent variables

$$X = \frac{v - \langle v\rangle}{\sigma_v}$$
$$Y = \frac{1}{\sqrt{1-\gamma^2}}\cdot\Big(\frac{p-\langle p\rangle}{\sigma_p} - \gamma\,X\Big). \tag{9}$$

Then, the random process in v and p is replaced by the sequence of two random processes in X and Y, respectively, with the moments

$$\langle X\rangle = \langle Y\rangle = \langle X\,Y\rangle = 0\,; \qquad \langle X^2\rangle = \langle Y^2\rangle = \tau. \tag{10}$$

The random processes are assumed to be Gaussians which can be treated easily within the numerical simulation. However, other random processes may be chosen just as well (see e.g. /10/). For Gaussian processes, the velocity space boundaries $v = 0$ as well as $|p| = 1$ must be handled with care since random numbers X and Y can lead to values $v < 0$ or $|p| > 1$ depending on the step size of Δt. This problem arises only for initial values v_i, p_i very close to the boundaries. On the one hand, the time step Δt can be strongly reduced in such a case; on the other hand, a new set of random numbers X, Y can be generated if $v < 0$ or $|p| > 1$ occurs. For this case, however, small deviations in the distribution functions very close to the boundaries are expected.

Now, the Monte Carlo scattering operator for the particle species α is given by the equivalent Gaussian random process

$$f^G = \frac{1}{2\pi v_i^2 \sigma_v \sigma_p \sqrt{1-\gamma^2}\,\tau} \cdot \exp\left(-\frac{X^2+Y^2}{2\tau}\right) \tag{11}$$

and the initial value problem

$$\lim_{\Delta t \to 0} f^G = \frac{1}{2\pi v_i^2 \sigma_v \sigma_p \sqrt{1-\gamma^2}\,\tau} \cdot \delta(X) \cdot \delta(Y) = \frac{1}{v_i^2} \cdot \delta(v - v_i) \cdot \delta(p - p_i)$$

where σ_v, σ_p and γ are defined by the equations (7) and the statistically independent variables X, Y are defined by the equations (9). From two independent Gaussian random numbers X and Y, random values of velocity, v, and pitch, p, are calculated corresponding to the diffusive nature of the Fokker-Planck collision term for each simulation particle. Due to parallel momentum conservation as described by the cross term in the Fokker-Planck equation (1), the random numbers v and p are not statistically independent. Energy and pitch angle scattering become statistically independent only in the case of an isotropic background plasma ($C = 0$).

The source function S_α in equation (1) is modelled by both generation and annihilation of simulation particles of species α. Corresponding to the specific physical problem, particle source operators S_α^+ as well as particle loss operators S_α^- must be constructed based on random processes.

IV. The Simulation Model

The H^o neutral beam injection in a D^+-H^+ plasma mixture for the case of good confinement properties (orbit losses neglected) is modelled by Monte Carlo simulation. Although no stationary conditions could be obtained under experimental conditions since the electron density inceases during the injection, the stationary distribut on function calculated in the simulation model is a good approximation as long as the average slowing-down time τ_{SD} is small compared to the particle confinement time τ_P. Due to the high

collision frequency, the electron distribution function is modelled by an isotropic Maxwellian with the measured value of the central electron temperature. Furthermore, the ion heat conduction is disregarded.

For the D^+ plasma component, no sources are assumed ($S_{D^+} = 0$). The generation of the H^+ simulation particles is approximated to the NBI in W VII-A by the formula:

$$S^+_{H^+} = \frac{1}{\sqrt{2\pi}\,\sigma_{NBI}} \cdot \exp\left(-\frac{(p - p_{NBI})^2}{2\,\sigma^2_{NBI}}\right) \cdot \sum_\nu w_\nu \cdot \frac{1}{v_\nu^2}\,\delta(v - v_\nu) \qquad (12)$$

with the mean pitch of the NBI, p_{NBI} (= 0.1, corresponding to 84^o injection angle), and the standard deviation, σ_{NBI} (= 0.035, corresonding to the divergence of the beam lines of $\pm 2^o$). v_ν are the velocities corresponding to the different injection energies with source strengths w_ν. For 27 kV voltage in W VII-A, the beam composition is assumed to be 21% : 32% : 47% for particles with 27, 13.5 and 9 keV energy. This particle source operator is statistically independent in v and p, the H^+ simulation particles being generated by means of two independent random processes.

To get stationary conditions, the loss strength is assumed to be equal to the source strength of the NBI. In a simple model, only thermalized particles are assumed to be lost, and the loss operator $S^-_{H^+}$ is defined by an isotropic Maxwellian. In the simulation, a random number v_L is generated (corresponding to the isotropic Maxwellian), and the H^+ simulation particle with v closest to v_L is annihilated. The temperature of the thermal part of the H^+ distribution function is equal to the deuterium temperature which is calculated self-consistently within the simulation by fitting a Maxwellian to the low energy part of the energy spectrum of the simulation particles.

As the Rosenbluth potentials (eqs. 3 and 4) depend strongly on the distribution functions, the Fokker-Planck equation (1) is nonlinear. Consequently, the scattering operators (eq. 11) depend on the H^+, D^+ distributions of the simulation particles, and the distributions must be calculated by means of iteration within the simulation. The time of an iteration step is of the order of the maximum slowing-down time for which the distributions of the simulation particles become constant. The time step Δt of the scattering operators (eqs. 8 and 11) as well as the source operators is very small compared to the collision times ($\simeq$ 10 μs). The distribution functions, f_{H^+} and f_{D^+}, averaged over the iteration time step, are used to calculate the Rosenbluth potentials (Appendix A1) and the expectation values (eqs. 7) for the next iteration step. This procedure is carried out until convergence is achieved. In Figure 1, the mean velocities, $< v >$, of the H^+ and D^+ simulation particles are plotted for the last 8 iteration steps. The H^+ and the D^+ distribution functions are each represented by 500 simulation particles. Time average within the iteration steps greatly improves the statistical accuracy.

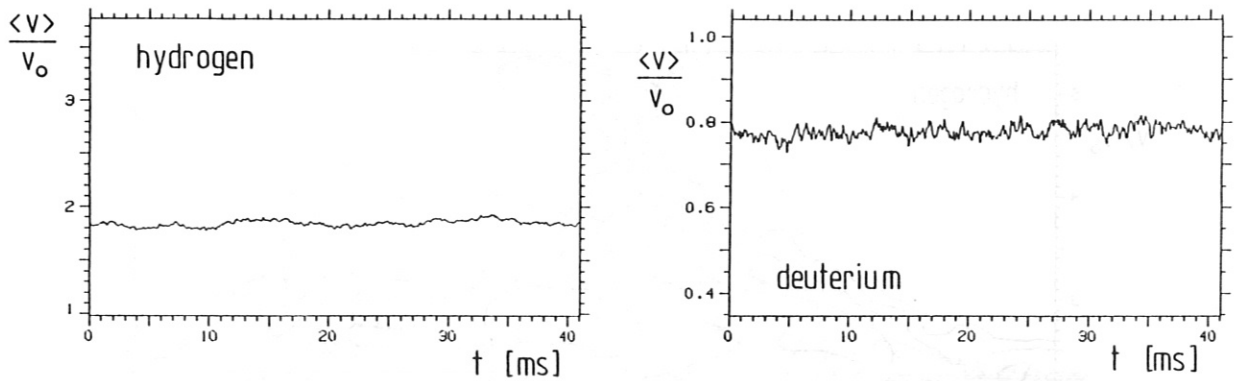

Fig. 1 *The mean velocity $< v >$ of the hydrogen and the deuterium simulation particles (normalized to the velocity v_o of 1 keV H^+) for the last 8 simulation steps. The time increment of the scattering operators is approximately 10 μs.*

The NBI model (eq. 12) includes an energy and a momentum source. With the assumption of a fixed Maxwellian distribution for the electrons, they act as a momentum sink. In addition most of the input power is transferred to the electrons. Thus, the self-consistently calculated ion temperature becomes larger than the electron temperature in this stationary model. As ion heat conduction and density increase are neglected, the calculated ion temperature is an upper limit compared to the experimental situation.

V. Results and Discussion

The Monte Carlo simulation, the results of which are now described in detail, was carried out for the following set of plasma parameters, which is typical for a neutral beam heated discharge in W VII-A with lower density:

electron temperature $T_e = 600\ eV$
electron density $n_e = 6.6 \cdot 10^{13}\ cm^{-3}$
deuterium density $n_{D^+} = 4.6 \cdot 10^{13}\ cm^{-3}$
(70% deuterium, 30% hydrogen plasma mixture)
27 kV voltage of NBI with 84^o injection angle
heating power density: $4.2\ W/cm^3$
(corresponding to 3 beam lines with 340 kW power absorbed)
resulting total source strength of H^+ : $1.85 \cdot 10^{15}\ cm^{-3}\ s^{-1}$.

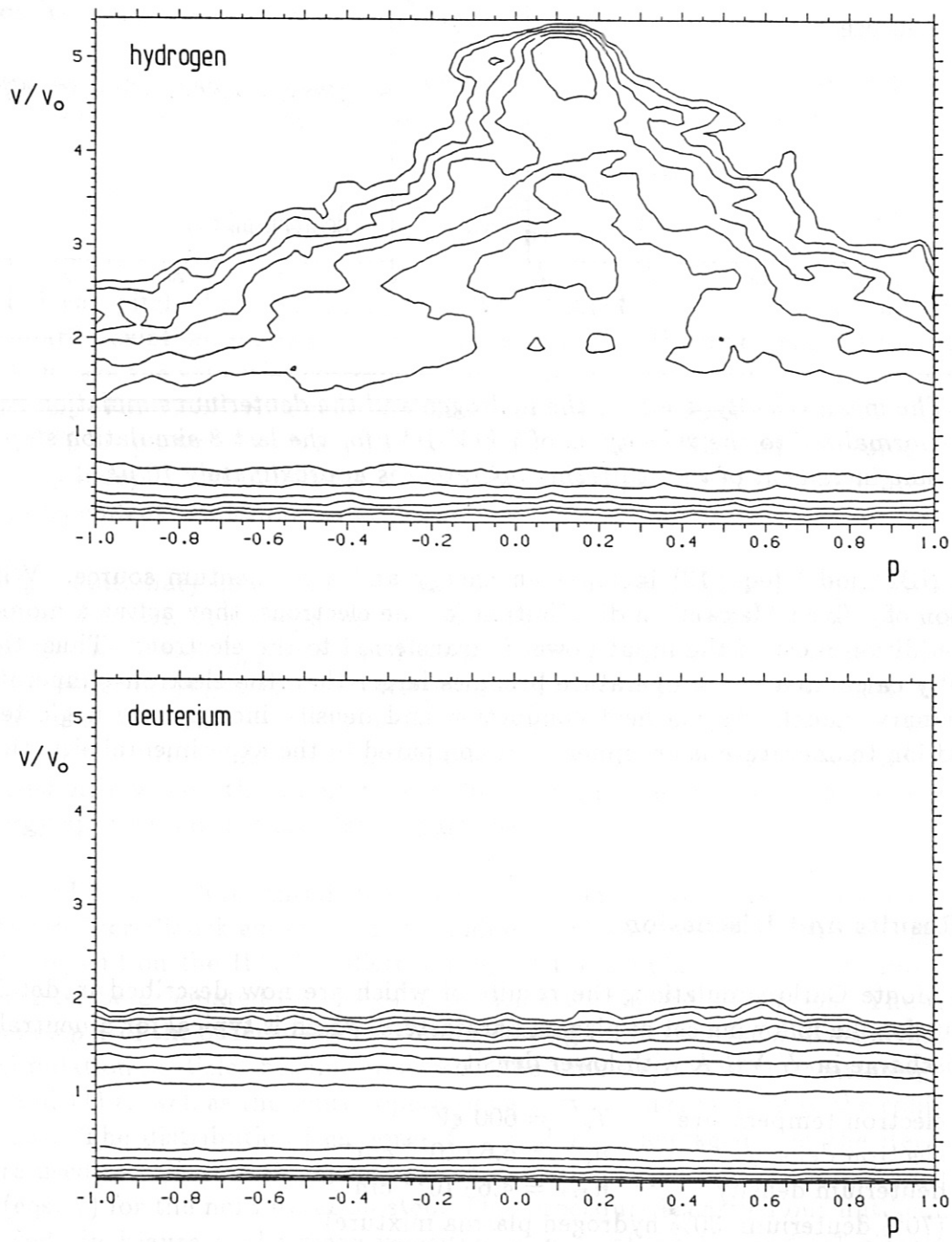

Fig. 2 *Isolines of the hydrogen and deuterium distribution functions, $v^2 \cdot f_{H^+}(v,p)$ and $v^2 \cdot f_{D^+}(v,p)$, in the velocity space, $(v,\ p)$, estimated from the number of simulation particles in the velocity space mesh averaged in time for the last simulation step.*

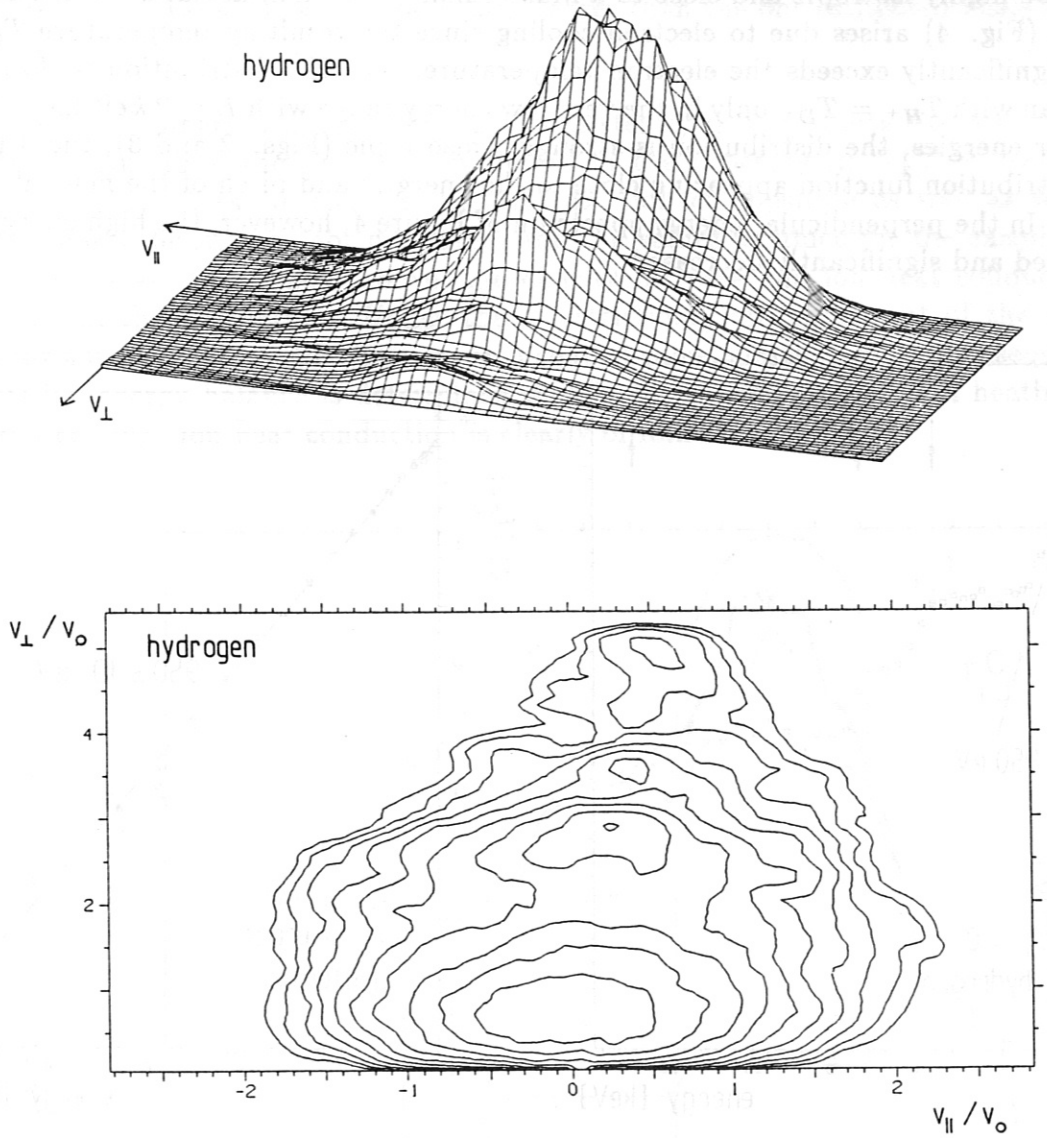

Fig. 3 *Isolines and perspective plot of the hydrogen distribution function, $v_{\perp} \cdot f_{H^+}(v_{\parallel}, v_{\perp})$, in the velocity space, $(v_{\parallel}, v_{\perp})$, corresponding to the distribution function of Figure 2.*

In Figures 2 and 3, the hydrogen and deuterium distribution functions are plotted in the velocity spaces (v, p) and ($v_{\|}$, $v_{\perp}$), respectively. The deuterium distribution was found to be highly isotropic and close to a Maxwellian. The small deviation in the energy spectrum (Fig. 4) arises due to electron cooling since the resulting temperature $T_{D^+} = 950\ eV$ significantly exceeds the electron temperature. The H^+ distribution is close to a Maxwellian with $T_{H^+} = T_{D^+}$ only in the very low energy range with $E \leq 2\ keV$ (see Fig.4). For higher energies, the distribution is strongly anisotropic (Figs. 2 and 3), the 3 peaks in the distribution function appearing close to the energies and pitch of the neutral beam injection. In the perpendicular energy spectrum of Figure 4, however, the high energy tail is smoothed and significantly decreased.

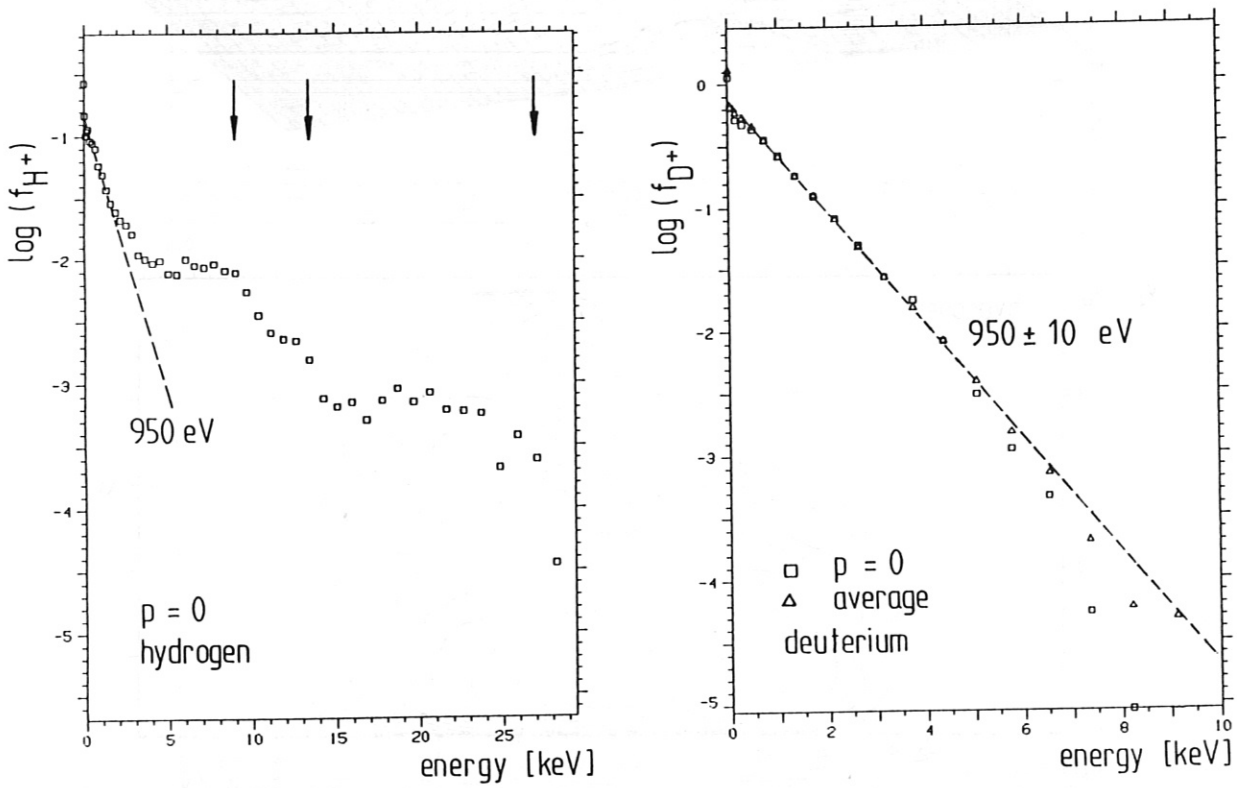

Fig. 4 *Perpendicular energy spectra of the hydrogen and deuterium distributions. The arrows in the figure on the left indicate the energies of the H^0 injection. In the right hand figure, the pitch-averaged spectrum (△) with higher statistical accuracy is also plotted.*

In the simulation, the strong NBI results in a total fraction of 13% non-thermal ions, which is related to a total pressure anisotropy of 35% with electrons included. The average parallel velocity of the H^+ distribution, however, is only 10% of the thermal velocity. The power balance for the H^+ component, normalized to the NBI input power, is as follows: 10% thermalization loss (density increase), 20% transfer to the D^+ component (which is lost to the electrons) and 70% power transfer to the electrons. This balance results from

the average over the H^+ distribution. The average slowing-down time, τ_{SD}, defined by the non-thermal part of the ion density divided by the NBI source strength, was found to be 4.7 *ms*. This value of τ_{SD} is about 20% larger than the one estimated analytically (for the formula see /3/).

The D^+ temperature, calculated self-consistently in the Monte Carlo simulation, is slightly greater than the central value found in the experiment: $T_{D^+}^{exp} = 850\ eV$ (CX-diagnostic). For these discharges, the H^+ / D^+ ion composition as well as the central heating power density are not measured, and the values assumed for the calculations are a little uncertain. As stated above, the density increase and ion heat conduction were neglected in the simulation. Under these restrictions, the agreement of the calculated deuterium temperature with the measured central value is rather good. Consequently, the central ion energy balance is determined mainly by the collisional beam heating and by electron cooling. Ion heat conduction is clearly of minor importance.

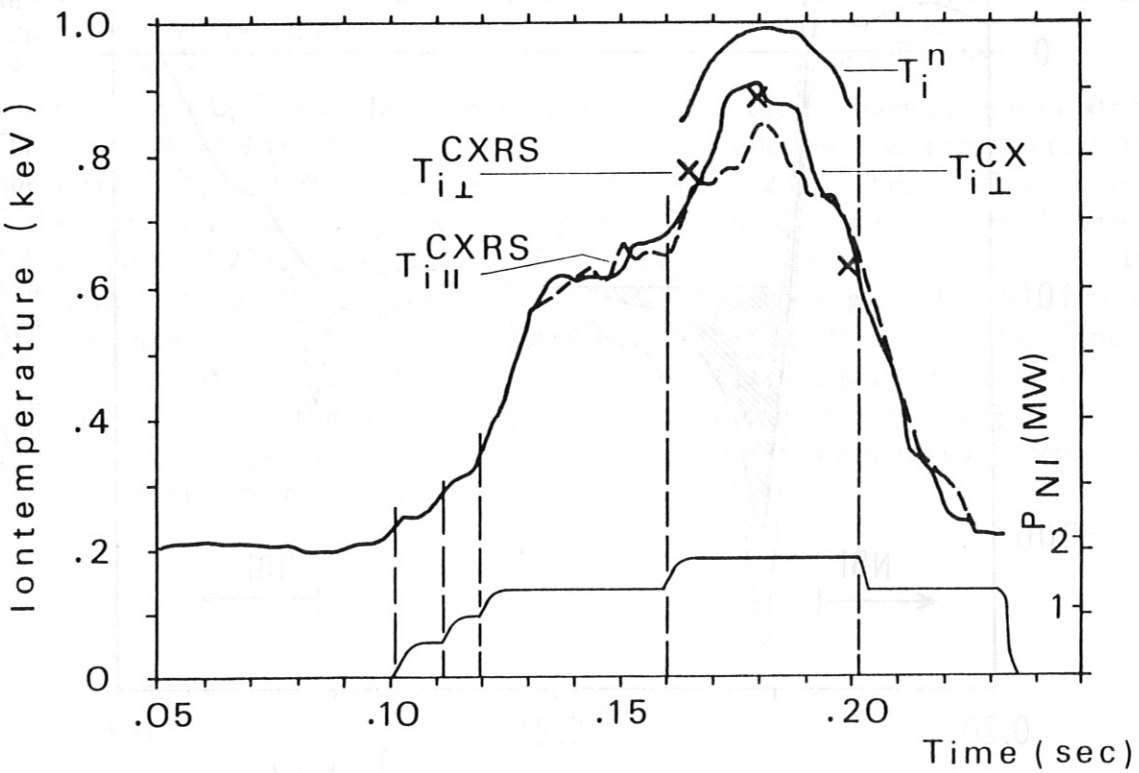

Fig. 5 *Ion temperatures T_i and injection power P_{NI} versus time for a discharge series in W VII-A. The temperature values are derived from the following diagnostics: energy analysis of charge exchange neutrals (CX), Doppler broadening of the O^{VIII} impurity line (CXRS), both parallel and perpendicular to the magnetic field, and neutron flux measurements (n) during D^o injection (4th injector).*

Some effort was made to confirm the deuterium temperature measured by charge exchange analysis, the results of which are plotted in Figure 5. The CX-temperature, $T_{i\perp}^{CX}$, measured perpendicular to the magnetic field, was evaluated from the flux of D^o neutrals generated in the central region (using a diagnostic injector) by energy analysis in the range $2\,T_i < E < 7\,T_i$. The T_i^{CXRS} values were estimated from Doppler broadening of the O^{VIII} impurity line (charge exchange resonance spectroscopy) both parallel and perpendicular to B, the energy range of evaluation being $E < 2\,T_i$. Finally, the temperature T_i^n is derived from the neutron flux of the D^+-D^+ reactions, the evaluation of which is based on the assumption of an isotropic Maxwellian for the deuterium distribution function. The agreement of all these ion temperature results is very good and confirms that the deuterium distribution function is very close to an isotropic Maxwellian.

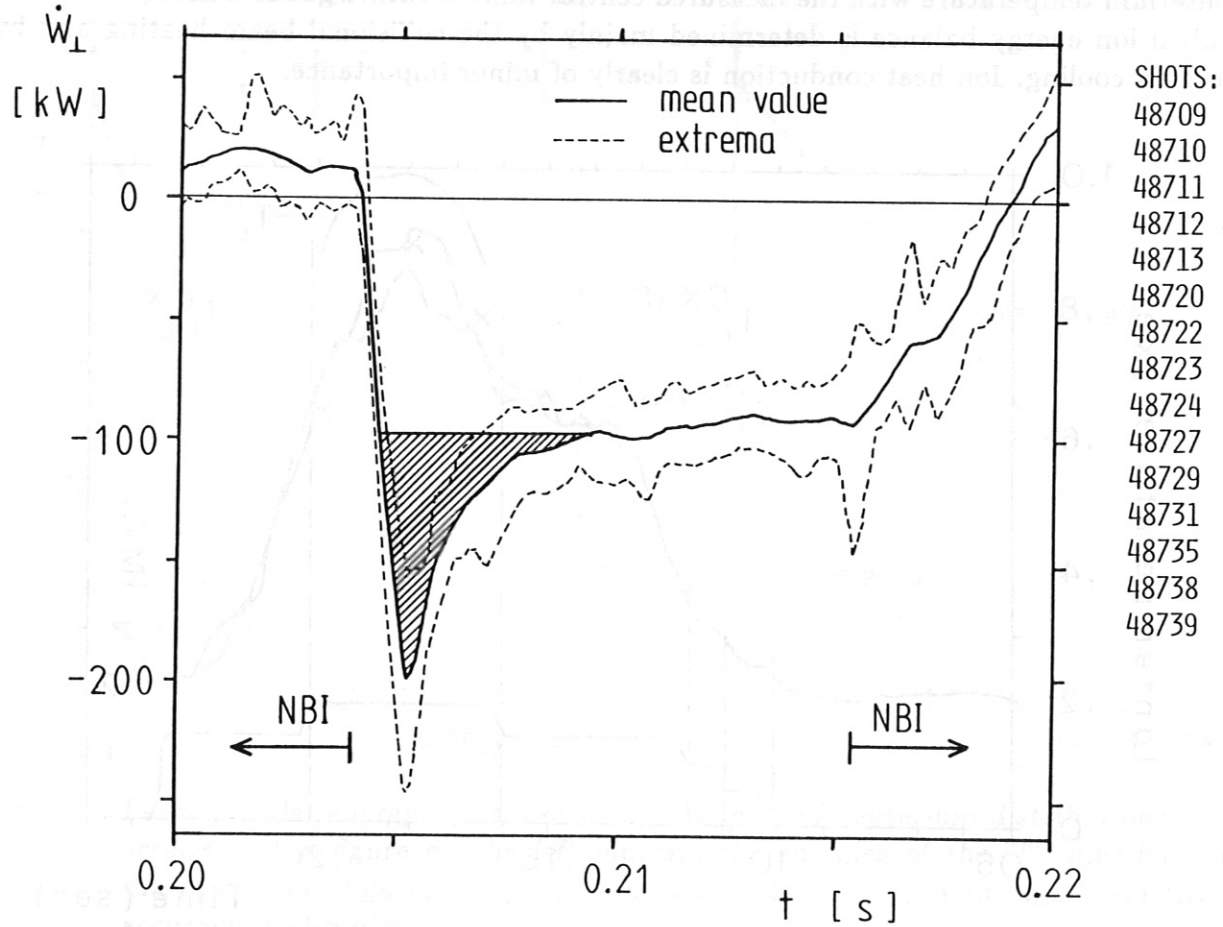

Fig. 6 *The internal energy production, $\dot{W}_\perp$, versus time when all neutral beam injectors (NBI) are switched off. The data are derived from the diamagnetic loop signals with a sampling frequency of about 3 kHz.*

An estimate of the pressure anisotropy averaged over the plasma column was derived from the diamagnetic signal after all injectors were switched off. The perpendicular component of the internal energy production, $\dot{W}_\perp$, is plotted in Figure 6. As the energy confinement time ($\simeq$ 12 ms) is much larger than the average slowing-down time ($\simeq 4ms$), the anisotropic part of the perpendicular energy component, which disappears nearly within a slowing-down time, can be separated from the thermal part. With the ansatz $\dot{W}_\perp = \dot{W}_\perp^{th} + \Delta\dot{W}_\perp$, where $\dot{W}_\perp^{th}$ is the thermal part, the perpendicular non-thermal component of the energy content, $\Delta W_\perp$, is estimated by integration in time (hatched area in Fig. 6) after switch-off of all injectors. Then, the pressure anisotropy averaged over the plasma cross-section is defined by $\Delta W_\perp / W_\perp^{th}$. For the discharges of Figure 6, an averaged pressure anisotropy of 13% was estimated. Here, the central plasma parameters are different from those used for the simulation, resulting in a shorter slowing-down time. For larger radii, the collisionality is increased and the slowing-down time decreased, and for the lower densities, the NBI deposition is smaller. Furthermore, the fast particle losses become more important near the plasma edge. Thus, the energy content $\Delta W \simeq \Delta W_\perp$ of the slowing-down distribution evaluated from the diamagnetic signal yields a lower limit for the central pressure anisotropy.

Figure 7 shows the perpendicular energy spectrum of the H^+ slowing-down distribution. The energy analysis of the CX-neutrals leads to the smoothed spectrum (points) since the energy resolution of the CX-analyser is of the order of 20%. These data are directly derived from the count rates; the energy dependence of the CX-cross section (decreasing σ_{CX} for $E > 10$ keV) is not taken into account. Therefore, the H^+ distribution function is closer to the calculated spectrum (solid curve) for higher energies. The Monte Carlo simulation is analogous to that outlined above except that the D^+ distribution function was assumed to be Maxwellian with the measured central ion temperature of 850 eV. The perpendicular flux, proportional to $v_\perp \cdot f_{H^+}$, was evaluated in the pitch range $|p| \leq 0.033$ corresponding to $\pm 2^o$ aperture. The distribution function is very sensitive in pitch (comp. Fig. 3), thus the agreement with the CX-data is rather good.

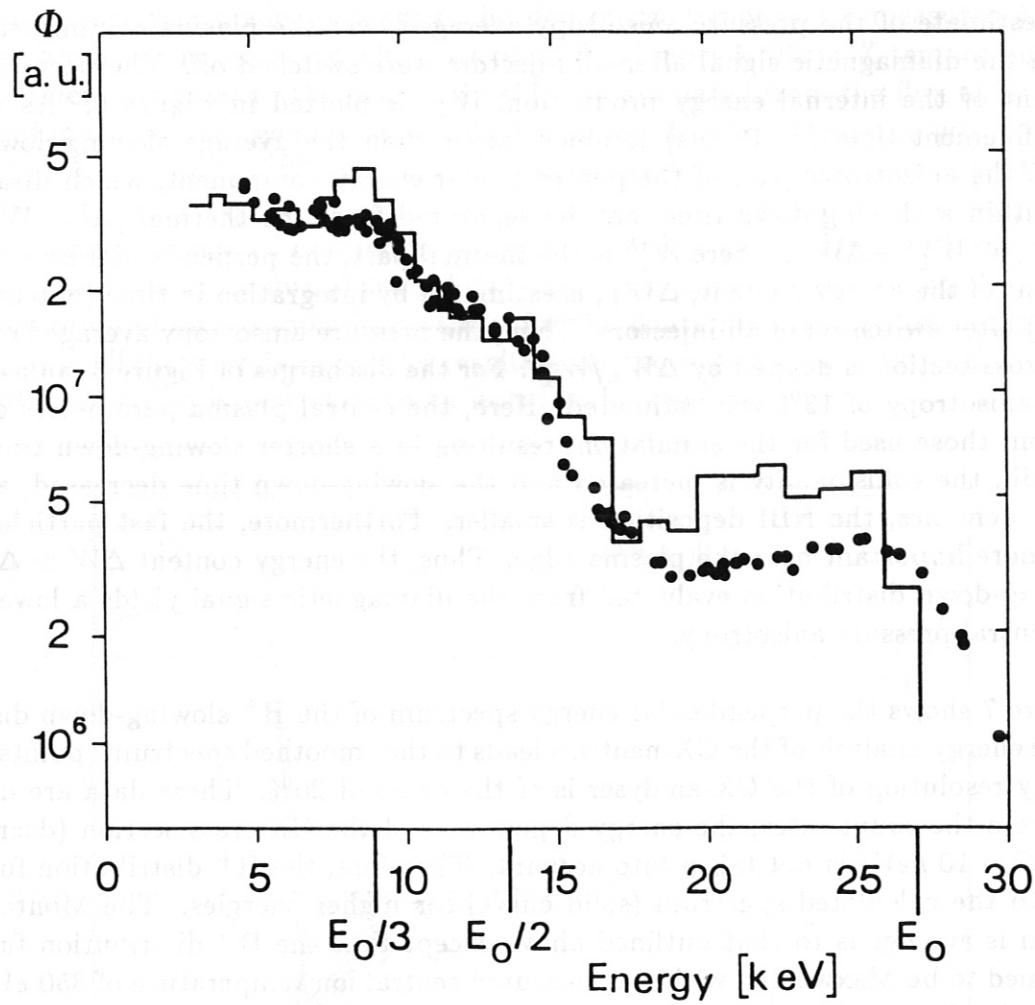

Fig. 7 *The perpendicular energy spectrum of the charge exchange H^o neutrals (dots) and the perpendicular flux, $v_\perp \cdot f_{H^+}$, calculated by Monte Carlo simulation (solid curve). For the simulation, the following central values of the plasma parameters have been used: $n_e = 6.6 \cdot 10^{13}\ cm^{-3}$, $T_e = 600\ eV$, $T_i = 850\ eV$.*

VI. Conclusions

The Monte Carlo simulation is a suitable technique to solve the nonlinear Fokker--Planck equation. Scattering operators for Coulomb interactions were found for arbitrary distribution functions of the plasma species. For the conditions of neutral beam heated discharges in the W VII-A stellarator, however, the nonlinearity in the Fokker-Planck collision term is relative small, and the D^+ plasma component is nearly unaffected by the high energy H^+ distribution of the injection. Furthermore, the collisions between the non-thermal H^+ particles result in a broadening of the high energy tail of the H^+ distribution function since the effect of pitch angle scattering due to the electrons is relative small. Newertheless, simplified scattering operators based on Maxwellian distribution functions are a relatively good approach under the conditions typical for W VII-A.

A strong pressure anisotropy was deduced from the diamagnetic loop signal for all injectors switched off. The lower limit of this anisotropy, averaged over the plasma column, is in qualitative agreement with the results derived from the Monte Carlo simulation. Furthermore, the calculated perpendicular energy spectrum of the H^+ slowing down distribution fits very well with charge exchange data. Together with neutron flux measurements in the case of deuterium injection, these results confirm the collisional slowing-down of the neutral beam injected particles.

Acknowledgements

The experimental investigations were a common effort of the W VII-A Team. Particularly, the author would like to thank Dr. J. Junker and Dr. M. Kick (CX flux measurements) and Dr. H. Renner (diamagnetic signal) for helpful discussions. The author thanks also W. von Zeppelin for his numerical support and Prof. Dr. M.A. Hellberg for his correct proofs of the final version.

Appendix

A1 Calculation of the Rosenbluth Potentials

For all distribution functions $f_\beta(v,p)$ estimated in the simulation, the Rosenbluth potentials h_α and g are calculated as outlined in the following. The contribution of all plasma species β can be separated:

$$h_\alpha = \sum_\beta Z_\beta^2 \, (1 + \frac{m_\alpha}{m_\beta}) \, H_\beta$$

$$g = \sum_\beta Z_\beta^2 \, G_\beta .$$

The distribution functions f_β, as well as the Rosenbluth potential contributions H_β and G_β are expanded in Legendre polynomials

$$f_\beta(v,p) = \sum_n f_\beta^n(v) \; P_n(p)$$

$$H_\beta(v,p) = \sum_n H_\beta^n(v) \; P_n(p)$$

$$G_\beta(v,p) = \sum_n G_\beta^n(v) \; P_n(p).$$

The Legendre coefficients H_β^n and G_β^n are calculated from the Green's function formula (eq.4):

$$H_\beta^n(v) = \frac{4\pi}{2n+1} \int_0^\infty \Gamma_H(v,v') \; f_\beta^n(v') \; dv'$$

$$G_\beta^n(v) = -\frac{4\pi}{4n^2-1} \int_0^\infty \Gamma_G(v,v') \; f_\beta^n(v') \; dv'$$

with $$\Gamma_H(v,v') = \min \left\{ \frac{v'^{n+2}}{v^{n+1}} \; ; \; \frac{v^n}{v'^{n-1}} \right\}$$

$$\Gamma_G(v,v') = \min \left\{ \frac{v'^{n+2}}{v^{n-1}} \left(1 - \frac{n - \frac{1}{2}v'^2}{n + \frac{3}{2}v^2}\right) ; \frac{v^n}{v'^{n-3}} \left(1 - \frac{n - \frac{1}{2}v^2}{n + \frac{3}{2}v'^2}\right) \right\}.$$

Within the numerical iteration, the distribution functions f_β are estimated from the ensembles of simulation particles. Depending on the number of simulation particles as well as on the number of steps for the time average, up to 40 polynomials are used in the Legendre expansion. Statistical deviations in the distribution functions have very little influence on the Rosenbluth potentials (smoothing by the velocity space convolution).

The derivatives of the Rosenbluth potentials in equation (2) are calculated directly: derivatives in v by convolution with the corresponding derivatives of the Green's functions, Γ_H and Γ_G, and derivatives in p by means of recurrence relations in the Legendre

summation. This procedure yields improved accuracy in the evaluation of the coefficient functions in the Fokker-Planck equation.

A2 Coefficient Functions for Maxwellian Plasma

If the distribution functions of all plasma species are isotropic Maxwellians, the Rosenbluth potentials are calculated analytically from equation (4). Straightforward integration yields:

$$h_\alpha^M = \frac{1}{v} \sum_\beta n_\beta Z_\beta^2 \, (1 + \frac{m_\alpha}{m_\beta}) \, \mathrm{erf}(v_\beta)$$

$$g^M = \sum_\beta n_\beta Z_\beta^2 \, \{(1 + \frac{1}{2v_\beta^2}) \, \mathrm{erf}(v_\beta) + \frac{v_{th_\beta}}{\sqrt{\pi}} \exp(-v_\beta^2)\}$$

with $v_\beta = v/v_{th_\beta}$ where v_{th_β} is the thermal velocity of the particle species β. Then, the coefficient functions of the Fokker-Planck equation defined in equation (2) are given by

$$A_1^M = \sum_\beta n_\beta Z_\beta^2 \, \{(1 + \frac{m_\alpha}{m_\beta}) \, \eta(v_\beta) - \overline{\eta}(v_\beta)\}$$

$$A_2^M = \sum_\beta n_\beta Z_\beta^2 \, \frac{v_{th_\beta}}{v_\beta} \, \eta(v_\beta)$$

$$B_1^M = \frac{p}{v} \sum_\beta n_\beta Z_\beta^2 \, \overline{\eta}(v_\beta)$$

$$B_2^M = \frac{1 - p^2}{v} \sum_\beta n_\beta Z_\beta^2 \, \overline{\eta}(v_\beta)$$

$$C^M = 0$$

with

$$\eta(x) = \mathrm{erf}(x) - \frac{2}{\sqrt{\pi}} x \, \mathrm{e}^{-x^2}$$

$$\overline{\eta}(x) = \mathrm{erf}(x) - \frac{1}{2x^2} \, \eta(x).$$

In the Monte Carlo simulations described in Chapter IV, the electron distribution function was assumed to be Maxwellian, and the electron contribution to the Coulomb scattering of the plasma ions was estimated from the corresponding part of these coefficient functions.

References

/1/ W VII-A Team, NI Group; *Proc. 10th Int. Conf. on Plasma Physics and Controlled Nuclear Fusion Research, London 1984, Nucl. Fusion Suppl., Vol. 2, p. 371, (1985)*

/2/ G. Grieger, et. al.; *Confinement of Stellarator Plasmas, Plasma Physics and Controlled Fusion, Vol. 28-1A, (1986)*

/3/ A. Weller and H. Maaßberg; *Neutron Flux Measurements at the Wendelstein VII-A Stellarator, Max-Planck-Institut für Plasmaphysik, Garching, Rep. IPP 2/278, (1985)*

/4/ W VII-A Team and NI Team; *5th Int. Workshop on Stellarators, Proc. of the IAEA Technical Committee Meeting on Plasma Confinement and Heating in Stellarators, ECSC-EEC-EAEC, EUR 9618 EN, Vol. 1, p. 179, (1984)*

/5/ H. Maaßberg and M.A. Hellberg; *Proc. (Contr. papers) Int. Conf. on Plasma Physics, Lausanne, p. 55, (1984)*

/6/ H. Maaßberg; *5th Int. Workshop on Stellarators, Proc. of the IAEA Technical Committee Meeting on Plasma Confinement and Heating in Stellarators, ECSC-EEC-EAEC, EUR 9618 EN, Vol. 2, p. 507, (1984)*

/7/ W VII-A Team and NI Team; *5th Int. Workshop on Stellarators, Proc. of the IAEA Technical Committee Meeting on Plasma Confinement and Heating in Stellarators, ECSC-EEC-EAEC, EUR 9618 EN, Vol. 1, p. 219, (1984)*

/8/ J. Killeen and K.D. Marx; *Methods in Computational Physics, Academic Press, Vol. 9, p. 421, (1970)*

/9/ J. Killeen, A.A. Mirin and M.E. Rensink; *Methods in Computational Physics, Academic Press, Vol. 16, p. 389, (1976)*

/10/ A.H. Boozer and G. Kuo-Petravic; *Phys. Fluids, Vol. 24, p. 851, (1981)*

/11/ W. Lotz and J. Nührenberg; *Z. Naturforsch., Vol. 37a, p. 899, (1982)*

/12/ H. Wobig; *Z. Naturforsch., Vol. 37a, p. 906, (1982)*

/13/ G.G. Lister, D.E. Post and R. Goldston; *Computer Simulation of Neutral Beam Injection into Tokamaks using Monte Carlo Techniques, 3. Symp. on Heating in Toroidal Plasmas, Varenna 1974, p. 303, (1974)*

/14/ M.N. Rosenbluth, W.M. MacDonald and D.L. Judd; *Phys. Rev., Vol. 107, p. 1, (1957)*